Flow Regime Maps and Optimization Thereby of Hydrodynamic Cavitation Reactors

Peeush Kumar
Dept. of Chemical Engineering, Indian Institute of Technology Guwahati, Guwahati 781 039, Assam, India

Swati Khanna
Center for Energy, Indian Institute of Technology Guwahati, Guwahati 781 039, Assam, India

Vijayanand S. Moholkar
Dept. of Chemical Engineering and Center for Energy, Indian Institute of Technology Guwahati, Guwahati 781 039, Assam, India

DOI 10.1002/aic.13771
Published online February 23, 2012 in Wiley Online Library (wileyonlinelibrary.com).

Hydrodynamic cavitation reactors are known to intensify diverse physical and chemical processes. In this article, flow regime maps have been proposed that give an overview of the operation of hydrodynamic cavitation reactor for different combinations of design and process parameters. These maps are based on simulations of cavitating flow using mathematical model that couples continuum mixture model with diffusion limited model. Specific flow regimes have been identified depending on the energetics of the collapse of cavitation bubble as sonophysical, sonochemical, and stable oscillatory (no physical or chemical effect). The radial motion of the bubble in the cavitating flow is governed by the mean and turbulent pressure gradients, which in turn, are decided by the design parameters. An analysis of variations in the pressure gradients in the cavitating flow with design parameters has been given. The flow regime maps form a useful tool for identification of most optimum set of design parameters for hydrodynamic cavitation reactor for a physical or chemical process. *AIChE J,* 58: 3858–3866, 2012
Keywords: cavitation, sonochemistry, process intensification, bubble dynamics

Introduction

Occurrence of physical or chemical change in a system is accompanied by energy transaction (either withdrawal or supply) across the system. For the transformations that require introduction of energy into the system, the method of energy introduction is a critical factor that governs the overall efficiency, and hence, viability and feasibility of the process. Among the new technologies, which have capability of introducing energy in the system in an efficient manner is the cavitation technology. In this technology, the cavitation phenomenon, that is, radial motion of a tiny gas/vapor bubble (comprising of nucleation, growth, and transient collapse) is used for producing the desired physical/chemical transformation. This radial motion (or volume oscillations) of the bubble are induced by variation of bulk pressure in the medium. Two simple means of varying the bulk pressure in a liquid medium are (1) passage of an ultrasound wave (in case of either stagnant or flowing medium) or (2) change of liquid velocity (in case of flowing medium) due to change in the flow geometry. The former method is known as acoustic cavitation, whereas the latter method is called hydrodynamic cavitation.

Research in the past two decades has demonstrated immense promise of hydrodynamic cavitation reactors for intensification of various physical and chemical processes such as degradation of dyes,[1] hydrolysis of oils,[2] degradation of recalcitrant pollutants and wastewater treatment,[3,4] nanosynthesis,[5,6] potable water disinfection,[7] and microbial cell disruption.[8,9] The literature on application of hydrodynamic cavitation for process intensification is quite vast and references cited above are only a few representative studies. The subject of modeling and optimization of hydrodynamic cavitation has been addressed by several authors. Moholkar and Pandit[10] and Moholkar et al.[11] reported simulations of single bubble in cavitating flow from orifice using linear pressure recovery, and linear pressure recovery with superimposed turbulent pressure fluctuations in the downstream region of orifice. Chatterjee and Arakeri[12] performed simulations of cavitating flow in a venturi to determine the maximum size of gas nuclei that would grow in the flow. Kumar and Pandit[13] have used the bubble cluster model of Morch for simulations of hydrodynamic cavitation in venturi tube and high speed homogenizer. Vichare et al.[14] and Kanthale et al.[15] have also used the cluster model for optimization of hydrodynamic cavitation in concurrence with experiments with a model sonochemical reaction. Gogate and Pandit[16] and Gogate et al.[17] have reported simulations of hydrodynamic cavitation reactors using a combination of models of Rayleigh–Plesset (for bubble wall Mach no. $\leq$ 1) and model of Tomita–Shima (for bubble wall Mach no. $>$ 1), and also

Additional Supporting Information may be found in the online version of this article.

Correspondence concerning this article should be addressed to V. S. Moholkar at vmoholkar@iitg.ernet.in.

have validated their results using Weissler reaction as the yardstick for cavitation yield and efficiency. Chatterjee[18] has reported experimental and numerical studies in controlling hydrodynamic cavitation in the shear layer downstream of a sudden expansion. Arrojo and Benito[19] have concluded that time scales of bubble motion in compression/rarefaction phase control the nature of bubble collapse. Larger time scales were found to hinder bubble collapse and reduce cavitation intensity. Sharma et al.[20] have modeled the reaction—diffusion kinetics of a cavitation bubble in flow downstream of an orifice. Mahulkar et al.[21] have investigated cavitation induced by injection of steam jet in subcooled water using numerical model for hydrodynamic cavitation. For greater details on literature on hydrodynamic cavitation, we refer to the reader to state-of-the-art reviews by Gogate[22,23] and Gogate and Pandit.[24,25]

Aim and approach of this study

Hydrodynamic cavitation can be generated by throttling discharge of a pump through constrictions such as a venturi or an orifice. In most of the literature on simulations of hydrodynamic cavitation reactors, a single and isolated bubble model has been used as basis. Thus, the bubble/bubble and bubble/flow interactions were ignored in most of the previous articles. In our earlier articles,[26,27] we had presented a unified model for hydrodynamic cavitation for both venturi as well as orifice configuration that took into account the bubble/bubble and bubble/flow interaction. This model was based on the continuum mixture model of van Wijngaarden[28,29] in which the nonlinear continuum model for bubbly mixture was coupled with Rayleigh–Plesset equation.[30,31] This model revealed interesting facets of cavitation bubble dynamics in both venturi and orifice flow configuration. It also gave an account of the influence of different design and process parameters on cavitation bubble dynamics, which formed useful guidelines and tools for design and optimization of hydrodynamic cavitation reactors. A major approximation in this model was neglection of the heat- and mass-transfer effects across bubble interface during the radial motion. More recently, we have addressed this important issue by extending the diffusion limited model of Toegel et al.[32] to hydrodynamic cavitation,[33–35] in which it was revealed that vapor transport across bubble interface was a major phenomenon affecting the cavitation bubble dynamics.

In this work, we have coupled the continuum mixture model to the diffusion limited model to study the dynamic behavior of cavitating flow downstream of an orifice. The new model reported in this article is more comprehensive and physically realistic in that it addresses all physical aspects of hydrodynamics of cavitating flow and the dynamics of the cavitation bubbles. This model takes into consideration the bubble/flow and bubble/bubble interaction, in addition to heat transfer and solvent vapor transport across bubble during radial motion. Another peculiarity of this work is that we have presented the results in the form of maps of flow regimes (represented by combination of design and process parameters) that characterize different types of bubble behavior, and thus, are useful in design and optimization of the hydrodynamic cavitation reactor for a particular physical or chemical process.

Mathematical Model

As stated earlier, the mathematical model of our study is based on coupling of the continuum mixture model of van Wijngaarden[28,29] to the diffusion limited model of Toegel et al.[32] Basic equations of both of these models along with background information has been given in the Supporting Information provided in this article. The two models are coupled through the bulk pressure term. An important module of the model is the estimation of turbulent fluctuation velocity downstream of the orifice. This velocity is superimposed over the mean flow velocity and gives rise to fluctuations in pressure gradient that ultimately influence the resultant bubble behavior. Calculation of the turbulent fluctuation velocity using Kolmogoroff's hypothesis is also explained in the Supporting Information provided in this article.[10] We have listed below the main equations of the steady-state bubble dynamics model that result after coupling of the continuum mixture model and diffusion limited bubble dynamics model. In case of cavitating flow in geometries such as an orifice plate, the mean flow parameters change rapidly in space and time due to acceleration/deceleration of the flow, and hence, the method of simple linearization is not applicable. Hence, we adopt the approach of Wang and Brennen,[30,31] based on the assumption of steady-state cavitating flow for a constant mass flow rate. In addition, we make two simplifying assumptions:

1. The mean flow expands linearly down stream of the orifice with flow area $A(x)$ written as

$$A(x) = A_o + \left(\frac{A_p - A_o}{L}\right) x \tag{1}$$

2. The steady-state frequency of the turbulent fluctuation velocity f_T (i.e., the total number of oscillations of the turbulent fluctuating velocity in the region of pressure recovery, $L = 8d_p$) is obtained by multiplying the rate of energy transfer ($\overline{u}'/l$) with the time of pressure recovery downstream of the orifice (t_{rec}), which is calculated using Newton's equations. The oscillatory nature of u' is approximated with a sinusoidal function ($u' = \overline{u}' \sin(2\pi f_T x/L)$), and thus, the instantaneous fluid velocity U is written as sum of mean (u) velocity (calculated using continuity Eq. A.4 given in Supporting Information) and turbulent fluctuating velocity

$$U = u + \bar{u}' \sin\left(\frac{2\pi f_T x}{L}\right) \tag{2}$$

We have chosen air–water system as the model system for our analysis, and hence, hereafter the word "solvent or liquid" refers to water while the word "gas" refers to air. At steady state, the bubble dynamics model is given by following set of equations

$$\rho_L(1 - 4\pi n R^3/3)uA = \text{constant} \tag{3}$$

$$U\frac{dU}{dx} = -\frac{1}{\rho_L(1 - 4\pi n R^3/3)}\frac{dp}{dx} \tag{4}$$

$$P_t = P_i - \frac{2\sigma}{R} - \frac{4\mu U}{R}\left(\frac{dR}{dx}\right) - \rho_L\left[R\left(U^2\frac{d^2R}{dx^2} + U\frac{dU}{dx}\frac{dR}{dx}\right) + \frac{3U^2}{2}\left(\frac{dR}{dx}\right)^2\right] \tag{5}$$

$$U\frac{dN_W}{dx} = 4\pi R^2 D_{ij}\frac{\partial C_W}{\partial r}\bigg|_{r=R} \approx 4\pi R^2 D_{ij}\left(\frac{C_{WR} - C_W}{l_{diff}}\right) \tag{6}$$

$$U\frac{dQ}{dx} = 4\pi R^2 \lambda\frac{\partial T}{\partial r}\bigg|_{r=R} \approx 4\pi R^2 \lambda\left(\frac{T_o - T}{l_{th}}\right) \tag{7}$$

Table 1. Range of Simulation Parameters

Parameter	Representative Values
1. Recovery pressure (P_2, kPa)	101.3 (1 atm), 202.6 (2 atm), 303.9 (3 atm)
2. Orifice to pipe diameter ratio (β)	0.3, 0.4, 0.5, 0.6
3. Cavitation number (C_i)	1.0, 1.1, 1.2
4. Initial bubble volume fraction (α)	1×10^{-8}, 2×10^{-8}, 1×10^{-7}, 2×10^{-8}

A pipe size of 0.0504 m or 2 in. ID and an initial size of 100 μm have been considered for all simulations. Liquid temperature is assumed to be 293 K or 20°C.

$$C_{v,mix}\frac{dT}{dx} = \frac{dQ}{dx} - P_i\frac{dV}{dx} + (h_W - U_W)\frac{dN_W}{dx} \tag{8}$$

Replacing p in Eq. 4 by P_t in Eq. 5 gives a system of six simultaneous differential equations which can be solved using Runge–Kutta fourth-order–fifth-order method with adaptive step size control[36] to get the radius history of the bubble along with instantaneous number of molecules trapped in the bubble and the temperature and pressure. The other physical properties of the flow are: density (ρ_L) = 1000 kg m^{-3}, surface tension (σ) = 0.072 N m^{-1}, and effective viscosity (μ) = 10^{-2} Pa s, so as to account for various mechanisms for damping of bubble oscillations.[37] The initial conditions used for the solution are: $x = 0$, $R = R_o = 100$ μm, $u = u_o$, $N_w = 0$, and $T = T_o = 293$ K. R_o is the initial (or equilibrium) radius of the bubble, which is difficult to measure experimentally. A typical range of the bubble sizes in hydrodynamic cavitation is 50–500 μm. We have chosen 100 μm as a representative value of this range.

For scanning of the parameter space for operation of hydrodynamic cavitation reactor, we have chosen three typical values of recovery pressure (P_2), four values for orifice to pipe diameter ratio (β), three values of cavitation number (C_i), and four values of the bubble volume fraction (α) generated at the vena contracta. These values have been listed in Table 1. Permutation–combination of these parameters gives 144 sets of operating conditions for which simulations have been carried out.

Criteria for mapping of flow regime and characterization of bubble motion

The flow regimes under different set of operating conditions were mapped on the basis of radial motion of the bubbles in the flow. The bubble motion was characterized in four categories: (1) stable oscillatory (OSC) inducing neither sonophysical (SP) nor sonochemical effect, (2) transient inducing SP effect, (3) transient inducing SP as well as sonochemical effect, and (4) indiscriminate expansion leading to flashing of the flow (Flash). In the OSC type motion, the expansion of the bubble during radial motion was less than 50% of its original size ($\geq 1.5R_o$) and the temperature in the bubble remained low (typically $\leq$ 400 K). For distinguishing between regimes of SP and sonochemical effects, we determined the minimum temperature (in the pressure range between 500 kPa and 100 MPa) at which the dissociation of H_2O will lead to formation of $^{\cdot}$OH radical. We selected $^{\cdot}$OH radical on the basis that it is the predominant radical species among all species formed after dissociation of water, and second, in most of the sonochemical reactions, $^{\cdot}$OH radicals play the dominant role in overall chemistry. We assumed thermal equilibrium to prevail in bubble throughout radial motion.[38] Using the software FACTSAGE that uses Gibbs energy minimization technique,[39,40] the temperature at which $^{\cdot}$OH radical formation commences (through dissociation of water molecules) was determined as $\geq$ 900 K. Thus, the sonochemical regime is characterized by strongly transient bubble motion with collapse temperature (T_{max}) $\geq$ 900 K, whereas the SP regime is characterized by moderately transient bubble motion with collapse temperatures in the range 400 K $\leq T_{max} \leq$ 900 K. Criteria for flashing has been explained in the next section.

Flow stability (or flashing) criterion

Consider two points, namely 0 and x downstream of orifice in the cavitating flow. Point 0 corresponds to the vena contracta, while x is any arbitrary location. We assume $C_i = 1$, so that pressure in the flow at vena contracta falls to vapor pressure of liquid. Applying Bernoulli equation between 0 and x, we get

$$P_x + \frac{1}{2}\rho u_x^2 = P_o + \frac{1}{2}\rho u_o^2 \tag{9}$$

Rearrangement gives

$$(P_x - P_o)/(\rho u_o^2/2) = 1 - (u_x/u_o)^2 = C_x \tag{10}$$

From continuity equation (Supporting Information, Eq. A4), we can write: u = constant/A $(1 - \alpha)$, which gives u_o = constant/A_o $(1 - \alpha_o)$ and u_x = constant/A_x $(1 - \alpha_x)$.

$\alpha(x,t) = \frac{4n\pi R^3(x,t)/3}{(1+4n\pi R^3(x,t)/3)}$ is the bubble volume fraction in the medium. Substituting for the velocities yields: $C_x = 1 - \left[\frac{(1-\alpha_o)A_o}{(1-\alpha_x)A_x}\right]^2$. Further, substituting for area ratio $A_o/A_x = \beta_x^2$ gives

$$C_x = 1 - \left[\frac{(1-\alpha_o)}{(1-\alpha_x)}\beta_x^2\right]^2 \tag{11}$$

It could be easily perceived that when bulk pressure in the flow downstream of orifice falls below vapor pressure leading to rapid expansion of the bubbles and vaporization of liquid. We call this phenomenon as "flashing of flow," which occurs for condition $C_x \leq 0$. This condition has been used to identify sets of design and process parameters, for which the flow downstream of the orifice flashes.

Results

Representative simulations of radial motion of cavitation bubble for each of four categories, namely flashing, moderately transient, strongly transient, and oscillatory, are depicted in Figures 1–3. The flow regime maps for oscillatory, moderately transient and strongly transient bubble motions for all four initial bubble volume fractions are given in Figures 4–6, respectively. These flow regime maps are essentially contour plots of cavitation number (which is a process parameter) against orifice to pipe diameter ratio and recovery pressure downstream of orifice, both of which are design parameters. Numerical results of entire 144 simulations (depicting the peak temperature attained during transient collapse and the characteristic bubble motion) have been given in Supporting Information, Table A.4–A.7.

The flow regime maps give an interesting account of relative impact of recovery pressure (P_2), orifice to pipe diameter ratio (β), and cavitation number (C_i), on the nature of the cavitating flow generated. Some general trends of bubble

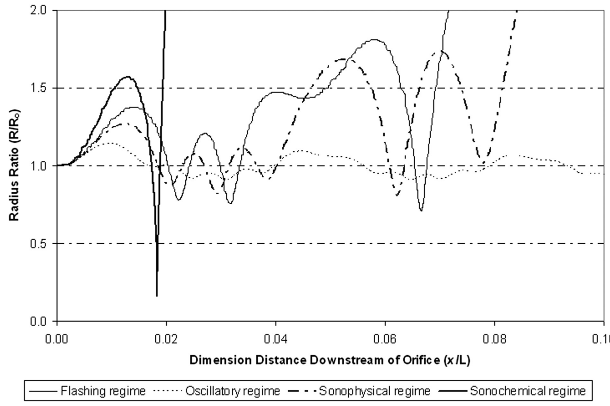

Figure 1. Simulation results: space variation of (dimensionless) radius of cavitation bubbles in different flow regimes.

Parameter set for flashing regime: P_2 = 202.6 kPa, C_i = 1, β = 0.6, $\alpha = 2 \times 10^{-7}$; parameter set for regime with moderately transient behavior: P_2 = 101.3 kPa, C_i = 1, β = 0.6, $\alpha = 1 \times 10^{-7}$; parameter set for regime with strongly transient behavior: P_2 = 303.9 kPa, C_i = 1, β = 0.3, $\alpha = 1 \times 10^{-7}$; parameter set for regime with oscillatory behavior: P_2 = 101.3 kPa, C_i = 1.1, β = 0.6, $\alpha = 2 \times 10^{-8}$.

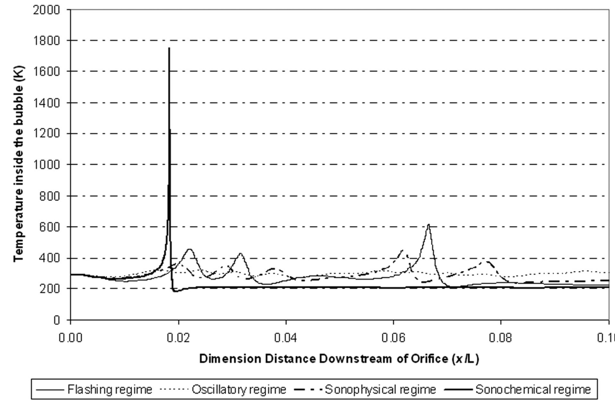

Figure 3. Simulation results: space variation of temperature inside the cavitation bubble in different flow regimes.

Parameter set for flashing regime: P_2 = 202.6 kPa, C_i = 1, β = 0.6, $\alpha = 2 \times 10^{-7}$; parameter set for regime with moderately transient behavior: P_2 = 101.3 kPa, C_i = 1, β = 0.6, $\alpha = 1 \times 10^{-7}$; parameter set for regime with strongly transient behavior: P_2 = 303.9 kPa, C_i = 1, β = 0.3, $\alpha = 1 \times 10^{-7}$; parameter set for regime with oscillatory behavior: P_2 = 101.3 kPa, C_i = 1.1, β = 0.6, $\alpha = 2 \times 10^{-8}$.

behavior for all values of α observed through the flow regime maps are as follows:

1. Oscillatory bubble behavior is seen for all values of α in entire range of recovery pressure, orifice to pipe diameter ratios > 0.35 and cavitation number > 1.1.

(2) Moderately transient bubble behavior is seen for C_i = 1 (or nearly 1) in entire range of recovery pressures and orifice to pipe diameter range of 0.4–0.6. However, for same cavitation number, for higher values of recovery pressure (202.6 or 303.9 kPa), the region of moderately transient bubble behavior is restricted for low values of orifice to pipe diameter ratio (< 0.4).

(3) The region corresponding to the strongly transient bubble behavior is more restricted, especially for higher bubble volume fractions of 1×10^{-7} and 2×10^{-7}. This region is bounded by C_i range 1–1.1 and orifice to pipe diameter range 0.4–0.6 for all values of recovery pressure.

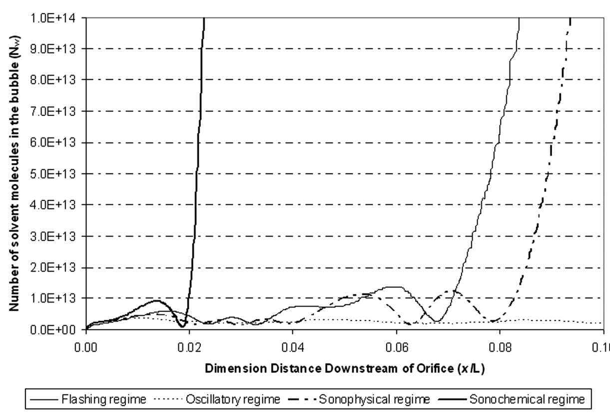

Figure 2. Simulation results: space variation of number of solvent (water) molecules in the cavitation bubble in different flow regimes.

Parameter set for flashing regime: P_2 = 202.6 kPa, C_i = 1, β = 0.6, $\alpha = 2 \times 10^{-7}$; parameter set for regime with moderately transient behavior: P_2 = 101.3 kPa, C_i = 1, β = 0.6, $\alpha = 1 \times 10^{-7}$; parameter set for regime with strongly transient behavior: P_2 = 303.9 kPa, C_i = 1, β = 0.3, $\alpha = 1 \times 10^{-7}$; parameter set for regime with oscillatory behavior: P_2 = 101.3 kPa, C_i = 1.1, β = 0.6, $\alpha = 2 \times 10^{-8}$.

The influence of the design and process parameters on cavitation bubble behavior as seen from the simulation results is summarized below.

Influence of orifice to pipe diameter ratio (β)

For all values of orifice to pipe diameter ratios considered in simulations, cavitation bubbles show only moderately transient behavior for C_i = 1 and P_2 = 101.3 kPa. This trend is consistent for all bubble volume fractions. As P_2 increases with cavitation number remaining the same, the bubble motion becomes more intense. For P_2 = 202.6 kPa and β = 0.6, flashing of the flow occurs for $\alpha = 1 \times 10^{-7}$ and 2×10^{-7}, whereas for β = 0.3, 0.4, and 0.5, the bubble undergoes a strong transient collapse giving sonochemical effect for all values of α. An interesting result is seen for $\alpha = 1 \times 10^{-8}$ and 2×10^{-8} at C_i = 1, the intensity of the bubble motion shows a minima at β = 0.5. As the recovery pressure increases to 303.9 kPa, the bubble motion becomes strongly transient for all values of α and β at C_i = 1.

Influence of cavitation number (C_i)

For all values of α at P_2 = 101.3 kPa and β = 0.3, the cavitation bubble shows moderately transient behavior at C_i = 1 and 1.1, whereas at C_i = 1.2, the bubble motion transforms into a small amplitude oscillatory type. This trend remains same for all values of α at higher recovery pressures of 202.6 and 303.9 kPa. With orifice to pipe diameter ratio rising to 0.4, the above behavior of cavitation bubbles stays the same for P_2 = 101.3 kPa; however, at higher recovery pressures (202.6 and 303.9 kPa), strongly transient behavior is seen for C_i = 1 and 1.1, whereas at C_i = 1.2, the bubble motion becomes moderately transient or oscillatory. This demonstrates that the influence of cavitation number on bubble behavior is sharper at higher recovery pressures. At β = 0.5 as well, it is seen that bubble behavior is moderately

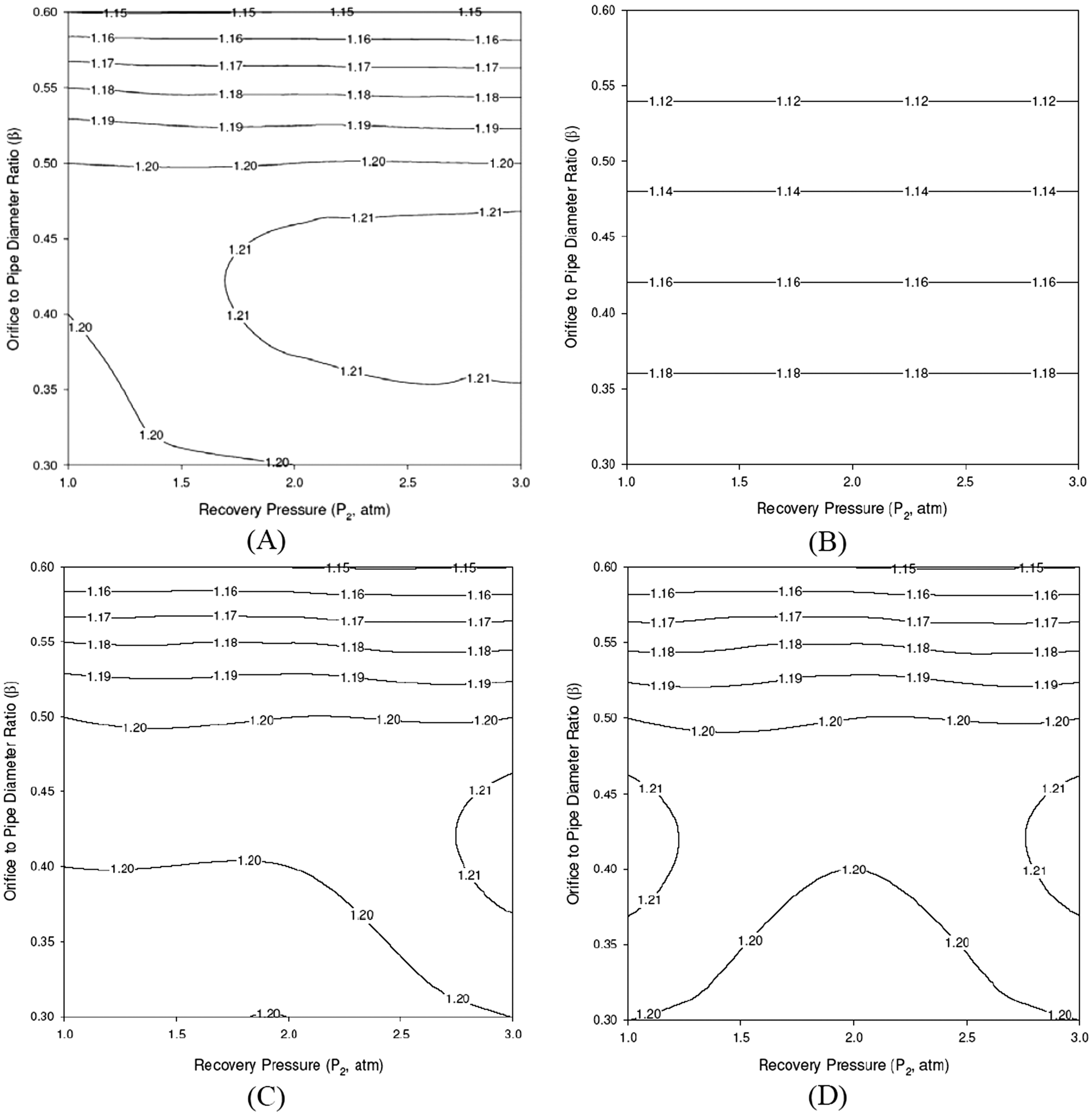

Figure 4. Flow regime maps (contour plots for the operating parameters) for oscillatory bubble behavior.

The lines inside the figure indicate contours for cavitation number (C_i). (A) Map for $\alpha = 1 \times 10^{-8}$; (B) map for $\alpha = 2 \times 10^{-8}$; (C) map for $\alpha = 1 \times 10^{-7}$; and (D) map for $\alpha = 2 \times 10^{-7}$.

transient at $C_i = 1$ and $P_2 = 101.3$ kPa for all values of α, and strongly transient at higher recovery pressures. The highest sensitivity of the flow behavior toward C_i for all values of α is seen at high recovery pressures of 202.6 or 303.9 kPa and $\beta = 0.6$. In this case, a sharp transition in radial motion of bubble is seen with small change in C_i, for example, from strongly transient behavior at $C_i = 1$ to oscillatory behavior at $C_i = 1.1$ or 1.2; or from flashing of the flow (at $\alpha = 1 \times 10^{-7}$ and 2×10^{-7}) for $C_i = 1$ to oscillatory behavior at $C_i = 1.1$ or 1.2.

Influence of recovery pressure (P_2)

The general trend in the bubble behavior with increasing P_2 at $C_i = 1$ for all values of α and β is that the bubble motion becomes more intense. However, there are some exceptions as follows: for $\alpha = 1 \times 10^{-7}$ and 2×10^{-7}, flashing of the cavitating flow occurs for $P_2 = 202.6$ kPa and $\beta = 0.6$, whereas at $P_2 = 101.3$ and 303.9 kPa strongly transient behavior is seen. With cavitation number rising to 1.1, the flow becomes stable (with no flashing) for all values of recovery pressures and orifice to pipe diameter ratios. At $P_2 = 202.6$ and 303.9 kPa and $C_i = 1.1$, the bubble motion is strongly transient for $\beta = 0.3$, 0.4, and 0.5. An interesting observation could be made for $\beta = 0.6$ at $C_i = 1.1$ as well as for all values of β at $C_i = 1.2$. For these conditions, the bubble motion is mostly of oscillatory type with few exceptions such as for combination of following parameters: (1) $P_2 = 101.3$ kPa, $\alpha = 2 \times 10^{-7}$, $\beta = 0.3$; (2) $P_2 = 303.9$ kPa, $\alpha = 2 \times 10^{-7}$, $\beta = 0.4$; (3) $P_2 = 101.3$ kPa, $\alpha = 1 \times 10^{-8}$, $\beta = 0.4$; (4) $P_2 = 303.9$ kPa, $\alpha = 1 \times 10^{-7}$, $\beta = 0.4$. This essentially means that the recovery pressure of the cavitating flow loses control over the radial motion of bubble for larger values of β and C_i.

Discussion

The trends shown by the flow regime maps can be interpreted on the basis of variation in pressure gradient in the cavitating flow that drives the radial motion of a bubble with the three parameters, namely P_2, β, and C_i. In an orifice flow, pressure recovery of the flow typically occurs within a distance of eight pipe diameters from vena contracta. The

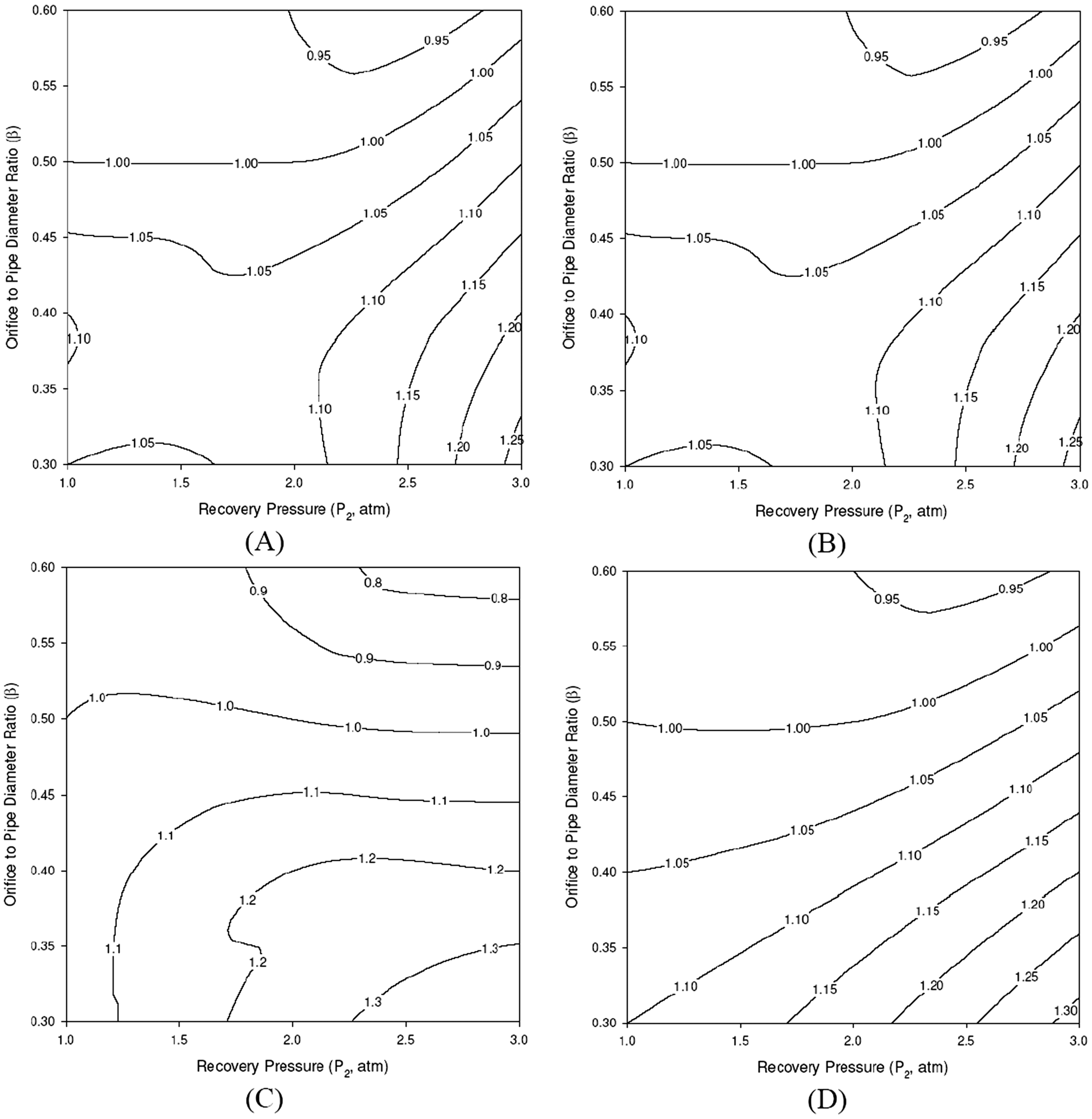

Figure 5. Flow regime maps (contour plots for the operating parameters) for moderately transient bubble behavior giving SP effects.

The lines inside the figure indicate contours for cavitation number (C_i). (A) Map for $\alpha = 1 \times 10^{-8}$; (B) map for $\alpha = 2 \times 10^{-8}$; (C) map for $\alpha = 1 \times 10^{-7}$; and (D) map for $\alpha = 2 \times 10^{-7}$.

mean pressure gradient at any location x can be determined from Eqs. 9–11 as

$$\frac{P_x - P_o}{x} \approx \frac{\rho u_o^2}{2x}\left(1 - \frac{u_x^2}{u_o^2}\right) = \frac{\rho u_o^2}{2x}\left[1 - \left(\frac{1-\alpha_o}{1-\alpha_x}\right)\beta_x^4\right] \approx \frac{\rho u_o^2}{2x}\left[1 - \left(\frac{1 + 4n\pi R_x^3/3}{1 + 4n\pi R_o^3/3}\right)\beta_x^4\right] \quad (12)$$

It could be perceived that larger expansion of the bubble would result in reduction of the mean pressure gradient. The second component of the pressure gradient is the turbulent pressure gradient which is proportional to the turbulent fluctuating velocity, $\overline{u}'$. The magnitude of this gradient can be written as $\sim \rho_L \overline{u}'^2/2$. The nature of these two pressure gradients is different, and so is the kind of influence they manifest on the radial motion of bubble. The mean pressure gradient is linearly increasing, and thus, it would not tend to grow a bubble above its original size at inception near vena contracta. Nonetheless, a larger mean pressure gradient will cause greater compression of the bubble. The turbulent pressure gradient is of oscillatory nature. During the negative oscillations, it would tend to reduce the mean pressure gradient causing growth of the bubble, with simultaneous evaporation of solvent vapor in it. Growth of the bubble would reduce the flow area causing rise in the velocity with reduction in mean pressure gradient, which in turn leads to further growth of the bubble. In the limiting situation, the mean pressure in the flow could fall below the vapor pressure causing flashing of the flow.

The type of radial motion that a bubble would undergo (whether small amplitude oscillatory, moderately transient, or strongly transient) in the cavitating flow depends on the relative magnitudes of the mean and turbulent pressure gradient. The magnitude of the mean pressure gradient depends on the cavitation number, recovery pressure, and the initial bubble volume fraction. For any combination of initial bubble volume fraction and recovery pressure, the largest mean pressure gradient occurs at $C_i = 1$. As C_i increases, the mean pressure gradient drops rapidly. The magnitude of turbulent pressure gradient depends on $\overline{u}'$, which varies

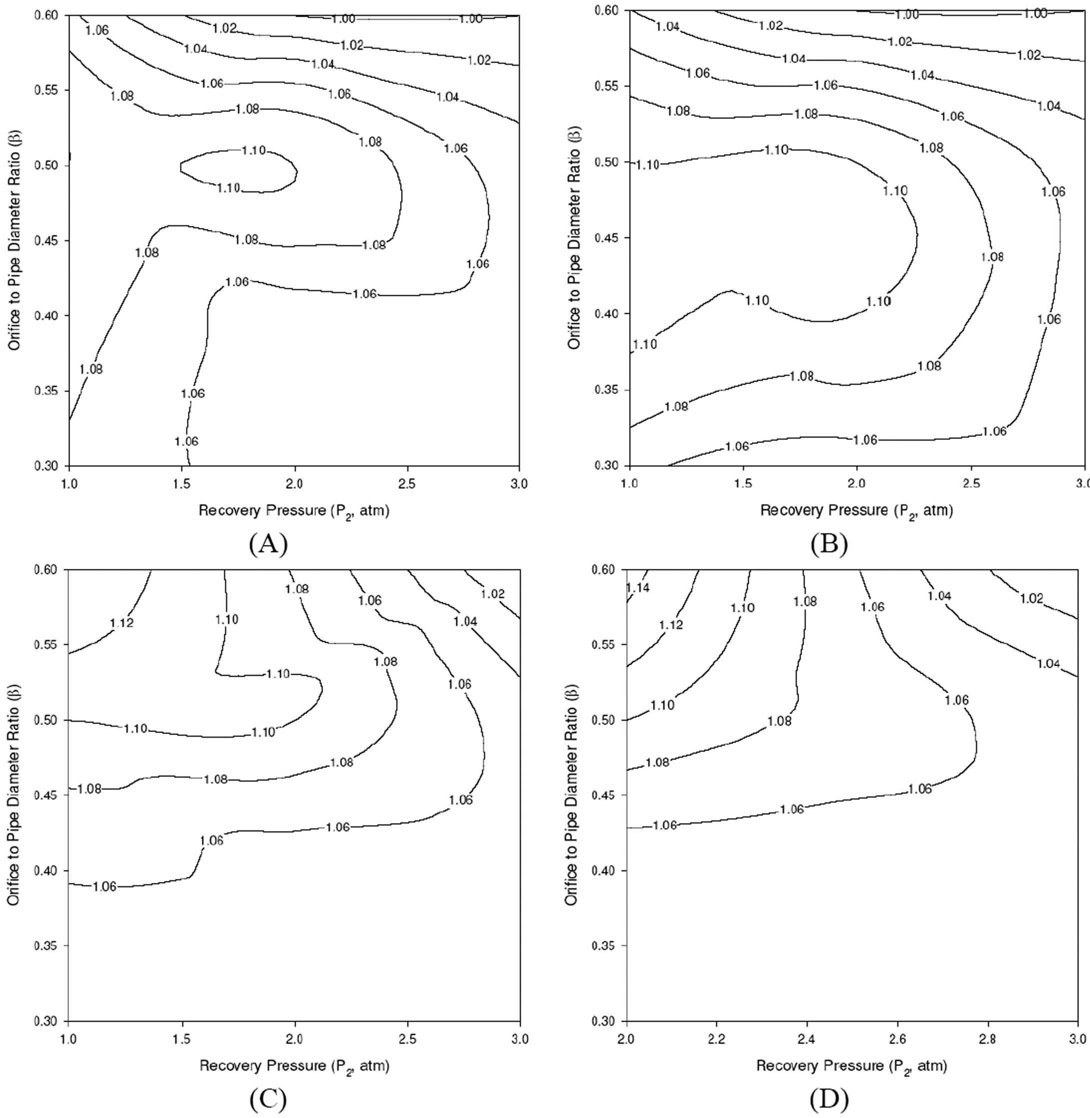

Figure 6. Flow regime maps (contour plots for the operating parameters) for strongly transient bubble behavior giving sonochemical effects.

The lines inside the figure indicate contours for cavitation number (C_i). (A) Map for $\alpha = 1 \times 10^{-8}$; (B) map for $\alpha = 2 \times 10^{-8}$; (C) map for $\alpha = 1 \times 10^{-7}$; and (D) map for $\alpha = 2 \times 10^{-7}$.

inversely with the orifice to pipe diameter ratio as well as cavitation number. For a bubble to undergo a strongly transient collapse, which would give rise to sonochemical effect, it needs to expand to at least twice of its original size followed by a rapid compression.[41] This would necessitate a moderate turbulent pressure gradient and high mean pressure gradient. If the turbulent pressure gradient is large and mean pressure gradient is moderate, the bubble collapse is only moderately transient due to large expansion of the bubble accompanied by significant vaporization of solvent. This solvent vapor cushions the bubble collapse reducing its intensity. Concurrent with this, we see strongly transient collapse at $C_i = 1$ for $P_2 = 101.3$ kPa and $C_i = 1$ or 1.1 at $P_2 = 202.6$ or 303.9 kPa. For combination of parameters $\beta = 0.3$, $C_i = 1$ and $P_2 = 101.3$ kPa, the bubble collapse is only moderately transient, as the large turbulent pressure gradient causes large expansion of the bubble with significant evaporation of water in it. Strongly transient collapse of vapor filled gas bubble would require high mean pressure gradient, which is not available for $P_2 = 101.3$ kPa.

For $C_i = 1.2$, both mean as well as turbulent pressure gradients are small. In such case, neither expansion nor compression of the bubble is appreciable, and the bubble essentially undergoes a small amplitude oscillatory motion in the flow. For large recovery pressure, for example, $P_2 = 303.9$ kPa, and large orifice-to-pipe diameter ratios ($\beta = 0.5$ or 0.6), combination of large mean pressure gradient and small turbulent gradient gives a moderately transient bubble collapse.

Comparison with experimental literature

In this section, we try to corroborate the bubble behavior predicted by the flow regime maps and its influence over the reaction system by citing results reported in some representative experimental studies. However, a direct quantitative comparison of results is not possible, as the flow configuration or geometry used by the authors is of different kind than that considered in this study. Most authors have used orifice plates, with multiple holes of given diameter arranged in a particular pattern. Moreover, the process parameters such as discharge pressure of pump, total open areas of orifice plate (equivalent to a single orifice), and cavitation numbers used in these studies are also beyond the range considered in our simulations. Even with these limitations, the qualitative trends in bubble behavior, as reflected in the experimental observations, could be compared with the flow regime maps.

1. Kumar et al.[42] observed that the rate of iodine liberation in Weissler reaction (oxidation of potassium iodide) reduces for too low values (< 0.06) of total fractional open area of orifice plate for a discharge pressure of 340 kPa. This is in concurrence with the region of sonochemical effect seen in contour maps in Figure 6, in which we do not see sonochemical effect (for cavitation number range 1–1.1) below orifice to pipe diameter ratio of 0.3.

2. Gogate et al.[17] have assessed efficiency of hydrodynamic cavitation with Weissler reaction as model. The cavitation yield (or extent of iodine liberation) increased with rising discharge pressure and reducing orifice to pipe diameter ratio. Although the exact values of cavitation numbers have not been reported in this study, the observed trend in result is seen in contour map of sonochemical effect which is bounded by low values of orifice to pipe diameter ratios and high discharge pressures.

3. Chakinala et al.,[43] Bremner et al.,[44] and Amin et al.[45] have reported optimization of hydrodynamic cavitation reactors for different types of reactions such as Weissler reaction in the presence of different chloroalkanes as additives, conversion of salicylic acid to 2,3- or 2,5-dihydroxy benzoic acid, and mineralization of 2,4 dichlorophenoxy acetic acid. All of these reactions are induced/accelerated by radicals generated from transient bubble collapse; especially the hydroxyl or $^{\cdot}OH$ radical. The extent of radical production through transient cavitation (by thermal dissociation of solvent vapor molecules entrapped in the bubble at transient collapse) varies directly with the temperature peak reached during collapse. The exact value of orifice to pipe diameter ratio (or fractional open area for flow) is not reported by authors, but for a constant value of this parameter the yield of above reactions increases with increasing discharge pressure (in the range of 3.4–10.3 MPa or 13.8–27.6 MPa), which essentially indicates increasing radical production with rising discharge pressure due to higher peak temperature reached in the bubble during transient collapse. This trend of peak temperatures at transient collapse of bubbles with discharge pressures is endorsed by our simulations. The flow regime maps show sonochemical effect for high recovery pressures. Thus, the experimental results of Chakinala et al.,[43] Bremner et al.,[44] and Amin et al.[45] are an indirect validation of the bubble behavior predicted by flow regime maps.

4. Pradhan and Gogate[3] have observed enhancement in degradation of *p*-nitrophenol with increasing discharge pressure (from 137 to 293.6 kPa) and reducing cavitation number (from 1.01 to 0.43). Similar observations have also been made by Mishra and Gogate[46] in degradation of Rhodamine-B dye. The degradation of organic pollutants is mediated by the OH radicals produced by transient collapse of cavitation bubble, which in turn is a direct function of temperature peak reached in the bubble during transient collapse, as mentioned above. Our simulations endorse the experimental trends observed in degradation of pollutants, in that temperature peak predicted by the model at transient bubble collapse increases with reducing cavitation number at a given discharge pressure. Moreover, for a given cavitation number, the temperature peak, and hence, the radical production also increases with increasing discharge pressure, as mentioned earlier.

Quite interestingly, the extent of degradation of the dye (or in other words, the cavitation yield) shows an optimum with respect to cavitation number, in that the degradation increases with cavitation number reducing from 0.161 (with discharge pressure of 294 kPa) to 0.099 (with discharge pressure of 490 kPa). Further reduction in cavitation number to 0.079 (at discharge pressure of 580 kPa) results in reduction of yield of degradation, which could be a consequence of uncontrolled growth of bubble resulting in local flashing of flow. As a result, the transient collapse of bubble does not occur, and hence, the radical production is reduced, which is manifested in reduced yield of degradation. This feature is also predicted by our simulations which show flashing of flow for combination of too low cavitation number and relatively high discharge pressure. Thus, the experimental results of Pradhan and Gogate[3] and Mishra and Gogate[46] are also a validation of the flow regime maps.

Conclusions

This study has put forward the flow regime maps for hydrodynamic cavitation reactor with orifice flow configuration using a model that takes into account bubble/bubble and bubble/flow interactions, in addition to the heat and mass transfer across bubble during radial motion. These maps give a vivid picture of the performance of the reactor under wide combinations of operating conditions. The principal physical phenomenon underlying intensification of any physical or chemical process by hydrodynamic cavitation reactor is the transient collapse of cavitation bubble causing local energy concentration. This study has demonstrated as how the radial motion of the cavitation bubble is influenced by the two pressure gradients, namely mean and turbulent, in the cavitating flow. In addition, the role of vapor transport across bubble interface is also discerned by the flow regime maps. The flow regime maps based on the simulations results depict the trends in nature of radial motion of cavitation bubbles (whether oscillatory, mildly transient or strongly transient) with design parameters. Among the three design parameters, namely recovery pressure, orifice-to-pipe diameter ratio and cavitation number, the characteristics of radial motion of bubble seem to be most sensitive to cavitation number. A small change ($\sim$20%) in this parameter can cause drastic change in the cavitation bubble motion. Most transient collapse of cavitation bubbles is seen for $C_i = 1$ (which is suitable for most physical and chemical processes), whereas for $C_i = 1.2$, the radial motion of cavitation bubble is of oscillatory type and practically ineffective for intensification of any process. Most optimum combination of parameters that gives energy intensive cavitation are: $P_2 = 202.6$ or 303.9 kPa, $\beta = 0.4$ or 0.5 and $C_i = 1$. The only parameter in the simulations, which is rather difficult to measure or control, is the initial bubble volume fraction (α) in the flow. The flow regime maps proposed in this study span over four typical values of α, and it could be perceived that the characteristics of the radial motion of bubble (for any combination of design parameters) are mostly independent of α, with exceptions of few cases where flashing of the flow has been observed. This result reduces the level of uncertainty in the use of flow regime maps (due to errors in estimating an accurate value of α). Summarizing, the flow regime maps presented in this article form a useful tool for design and optimization of the hydrodynamic cavitation reactor for any physical or chemical process.

Acknowledgments

The authors express their gratitude toward the two anonymous referees of this article for their meticulous assessment and constructive criticism of the manuscript and valuable suggestion for improvements in it.

Literature Cited

1. Wang J, Wang X, Guo P, Yu J. Degradation of Reactive Brilliant Red K-2BP in aqueous solution using swirling jet-induced cavitation combined with H_2O_2. *Ultrason Sonochem.* 2011;18:494–500.
2. Sainte Beuve R, Morison KR. Enzymatic hydrolysis of canola oil with hydrodynamic cavitation. *Chem Eng Process.* 2010;49:1101–1106.
3. Pradhan AA, Gogate PR. Removal of p-nitrophenol using hydrodynamic cavitation and fenton chemistry at pilot scale operation. *Chem Eng J.* 2010;156:77–82.
4. Kalumuck KM, Chahine GL. The use of cavitating jets to oxidize organic compounds in water. *J Fluids Eng.* 2000;122:465–470.
5. Pinjari DV, Pandit AB. Cavitation milling of natural cellulose to nanofibrils. *Ultrason Sonochem.* 2010;17:845–852.
6. Find J, Emerson SC, Krausz IM, Moser WR. Hydrodynamic cavitation as a tool to control macro-, micro-, and nano-properties of inorganic materials. *J Mater Res.* 2001;16:3503–3513.
7. Botha CJ, Buckley CA. Disinfection of potable water: the role of hydrodynamic cavitation. *Water Supply* 1995;13:219–229.
8. Balasundaram B, Harrison STL. Disruption of brewers' yeast by hydrodynamic cavitation: process variables and their influence on selective release. *Biotechnol. Bioeng.* 2006;94:303–311.
9. Balasundaram B, Pandit AB. Selective release of invertase by hydrodynamic cavitation. *Biochem Eng J.* 2001;8:251–256.
10. Moholkar VS, Pandit AB. Bubble behavior in hydrodynamic cavitation: effect of turbulence. *AIChE J.* 1997;43:1641–1648.
11. Moholkar VS, Kumar PS, Pandit AB. Hydrodynamic cavitation for sonochemical effects. *Ultrason Sonochem.* 1999;6:53–65.
12. Chatterjee D, Arakeri VH. Towards the concept of hydrodynamic cavitation control. *J Fluid Mech.* 1997;332:377–394.
13. Kumar PS, Pandit AB. Modeling hydrodynamic cavitation. *Chem Eng Technol.* 1999;22:1017–1027.
14. Vichare NP, Gogate PR, Pandit AB. Optimization of hydrodynamic cavitation using a model reaction. *Chem Eng Technol.* 2000;23: 683–690.
15. Kanthale PM, Gogate PR, Pandit AB, Wilhelm AM. Dynamics of cavitational bubbles and design of a hydrodynamic cavitational reactor: cluster approach. *Ultrason Sonochem.* 2005;12:441–452.
16. Gogate PR, Pandit AB. Engineering design methods for cavitation reactors II: hydrodynamic cavitation. *AIChE J.* 2000;46:1641–1649.
17. Gogate PR, Shirgaonkar IZ, Sivakumar M, Kumar PS, Vichare NP, Pandit AB. cavitation reactors: efficiency assessment using a model reaction. *AIChE J.* 2001;47:2526–2538.
18. Chatterjee D. Use of ultrasonics in shear layer cavitation control. *Ultrasonics.* 2003;41:465–475.
19. Arrojo S, Benito Y. A theoretical study of hydrodynamic cavitation. *Ultrason Sonochem.* 2008;15:203–211.
20. Sharma A, Gogate PR, Mahulkar A, Pandit AB. Modeling of hydrodynamic cavitation reactors based on orifice plates considering hydrodynamics and chemical reactions occurring in bubble. *Chem Eng J.* 2008;143:201–209.
21. Mahulkar AV, Bapat PS, Pandit AB, Lewis FM. Steam bubble cavitation. *AIChE J.* 2008;54:1711–1724.
22. Gogate PR. Cavitation: an auxiliary technique in wastewater treatment schemes. *Adv Environ Res.* 2002;6:335–358.
23. Gogate PR. Application of cavitational reactors for water disinfection: current status and path forward. *J Environ Manage.* 2007;85:801–815.
24. Gogate PR, Pandit AB. Hydrodynamic cavitation reactors: a state of the art review. *Rev Chem Eng.* 2001;17:1–85.
25. Gogate PR, Pandit AB. A review and assessment of hydrodynamic cavitation as a technology for the future. *Ultrason Sonochem.* 2005;12:21–27.
26. Moholkar VS, Pandit AB. Numerical investigations in the behavior of one-dimensional bubbly flow in hydrodynamic cavitation. *Chem Eng Sci.* 2001;56:1411–1418.
27. Moholkar VS, Pandit AB. Modeling of hydrodynamic cavitation reactors: a unified approach. *Chem Eng Sci.* 2001;56:6295–6302.
28. van Wijngaarden L. On the equations of motion for mixtures of liquid and gas bubbles. *J Fluid Mech.* 1968;33:465–474.
29. van Wijngaarden L. One dimensional flow of liquids containing small gas bubbles. *Ann Rev Fluid Mech.* 1972;4:369–396.
30. Wang Y-C, Brennen CE. One dimensional bubbly cavitating flows through a converging–diverging nozzle. *J Fluids Eng.* 1998;120: 166–170.
31. Wang Y-C, Brennen CE. Numerical computation of shock waves in a spherical bubble cloud of cavitation bubbles. *J Fluids Eng.* 1999; 121:872–880.
32. Toegel R, Gompf B, Pecha R, Lohse D. Does water vapor prevent upscaling sonoluminescence. *Phys Rev Lett.* 2000;85:3165–3168.
33. Krishnan JS, Dwivedi P, Moholkar VS. Numerical investigation into the chemistry induced by hydrodynamic cavitation. *Ind Eng Chem Res.* 2006;45:1493–1504.
34. Kumar KS, Moholkar VS. Conceptual design of a novel hydrodynamic cavitation reactor. *Chem Eng Sci.* 2007;62:2698–2711.
35. Kumar P, Moholkar VS. Numerical assessment of hydrodynamic cavitation reactors using organic solvents. *Ind Eng Chem Res.* 2011;50:4769–4775.
36. Press WH, Teukolsky SA, Flannery BP, Vetterling WT. *Numerical recipes*. New York: Cambridge University Press, 1992.
37. Chapman RB, Plesset MS. Thermal effects in the free oscillations of gas bubbles. *ASME J. Basic Eng.* 1971;93:373–376.
38. Brenner M, Hilgenfeldt S, Lohse D. Single-bubble sonoluminescence. *Rev Mod Phys.* 2002;74:425–484.
39. Eriksson G. Thermodynamic studies of high temperature equilibria. XII. SOLGAMIX, A computer program for calculation of equilibrium composition in multiphase systems. *Chem Scr.* 1975;8:100–103.
40. FactWeb. Homepage: http://www.factsage.com, accessed November 2009.
41. Flynn HG. Cavitation dynamics I. A mathematical formulation. *J Acoust Soc Am.* 1975;57:1379–1396.
42. Kumar PS, Kumar MS, Pandit AB. Experimental quantification of chemical effects of hydrodynamic cavitation. *Chem Eng Sci.* 2000;55:1633–1639.
43. Chakinala AG, Gogate PR, Chand R, Bremner DH, Molina R, Burgess AE. Intensification of oxidation capacity using chloroalkanes as additives in hydrodynamic and acoustic cavitation reactors. *Ultrason Sonochem.* 2008;15:164–170.
44. Bremner DH, Di Carlo S, Chakinala AG, Cravotto G. Mineralization of 2,4-dichlorophenoxyacetic acid by acoustic or hydrodynamic cavitation in conjunction with advanced Fenton process. *Ultrason Sonochem.* 2008;15:416–419.
45. Amin LP, Gogate PR, Burgess AE, Bremner DH. Optimization of a hydrodynamic cavitation reactor using salicylic acid dosimetry. *Chem Eng J.* 2010;156:165–169.
46. Mishra KP, Gogate PR. Intensification of degradation of rhodamine B using hydrodynamic cavitation in the presence of additives. *Sep Purif Technol.* 2010;75:385–391.

Manuscript received Aug. 15, 2011, and revision received Feb. 2, 2012.